Dissection of the Pathway of Molecular Recognition by Calmodulin†

James K. Kranz, Peter F. Flynn, Ernesto J. Fuentes,‡ and A. Joshua Wand*

The Johnson Research Foundation and Department of Biochemistry and Biophysics, University of Pennsylvania, Philadelphia, Pennsylvania 19104-6059

Received September 19, 2001; Revised Manuscript Received December 12, 2001

ABSTRACT: Amide hydrogen exchange has been used to examine the structural dynamics and energetics of the interaction of a peptide corresponding to the calmodulin-binding domain of smooth muscle myosin light chain kinase (smMLCKp) with calcium-saturated calmodulin. Heteronuclear NMR ^{15}N-^{1}H correlation spectroscopy was used to quantify amide proton exchange rates of the uniformly ^{15}N-labeled domain bound to calmodulin. A key feature of a proposed model for molecular recognition by calmodulin [Ehrhardt et al. (1995) *Biochemistry 34*, 2731−2738] is tested by examination of the dependence of amide hydrogen exchange on applied hydrostatic pressure. Hydrogen exchange rates and corresponding protection factors ($1/K_{op}$) for individual amide protons of the bound smMLCKp domain span 5 orders of magnitude at ambient pressure. Individual protection factors decrease significantly in a linear fashion with increasing hydrostatic pressure. A common pressure dependence is revealed by a constant large negative volume change across the residues comprising the core of the bound helical domain. The pattern of protection factors and their response to hydrostatic pressure is consistent with a structural reorganization that results in the concerted disruption of ion pairs between calmodulin and the bound domain. These observations reinforce a model for the molecular recognition pathway where formation of the initial encounter complex is followed by helix−coil transitions in the bound state and subsequent concerted formation of the extensive ion pair network defining the intermolecular contact surface between CaM and the target domain in the final, compact complex structure.

Calcium is a ubiquitous signal in eukaryotes that is both controlled and transmitted by a series of calcium-binding proteins, commonly referred to as EF-hand proteins. Calmodulin (CaM)[1] is a relatively small (148 amino acids) acidic protein that acts as a primary intracellular calcium sensor protein, regulating target proteins through protein−protein interactions in a calcium-dependent manner and ultimately transducing the initial Ca^{2+} signal into a wide range of cellular events and processes [for a review, see Crivici and Ikura (*1*)]. The association of calmodulin and its various targets of Ca^{2+}-regulated association are well studied, yet a mechanistic description of target activation is still confounded by the apparently diverse target sequences and numerous, often disparate, activities that are regulated by this protein (*1*−*4*).

The basic structural paradigm for calcium-dependent molecular recognition by calmodulin has been revealed by a series of crystallographic and NMR-based studies. In all states and complexes examined thus far, calmodulin is found to be composed of two structurally homologous globular domains. In the calcium-free state, each domain of calmodulin is comprised of a four-helix bundle and the two domains are bridged by a long helix that is dynamically disordered at its center (*5*, *6*). There are no significant contacts between the two globular domains. Upon binding calcium, each globular domain reorganizes its tertiary structure to form two helix−loop−helix or EF-hand motifs (*7*). This structural rearrangement exposes a large surface to solvent that will ultimately form extensive hydrophobic and ionic contacts with the target domain. Again, in the free but calcium-activated state, the two globular domains of calmodulin are tethered together by a bridging helix that is dynamically disordered at its center (*8*). The calmodulin-binding domains of proteins bound by calmodulin are generally composed of short basic and contiguous amphiphilic sequences (*4*). In the classic example of the interaction of the myosin light chain calmodulin-binding domain with calcium-saturated calmodulin, the two globular domains largely maintain the tertiary structure of the free calcium-activated state but pack around the small calmodulin-binding domain and support its formation of an α-helical structure (*9*−*11*). As with other protein−protein interfaces (*12*), the intermolecular interface involves extensive hydrophobic and polar interactions, including the so-called hydrophobic anchor residues of smMLCKp and their interactions with the hydrophobic patches of CaM. The peptide adopts an α-helical conformation when bound to CaM,

† Supported by NIH Grant DK39806 and by equipment grants from the NIH and the ARO. J.K.K. is the recipient of an NRSA fellowship (GM20206).

* Address correspondence to this author at the Department of Biochemistry and Biophysics, University of Pennsylvania, Philadelphia, PA 19104. Telephone: (215)-573-7288. Facsimile: (215)-573-7290. E-mail: wand@mail.med.upenn.edu.

‡ Present address: Department of Biochemistry and Biophysics, University of North Carolina, Chapel Hill, NC 27599.

[1] Abbreviations: Bis-Tris, bis(2-hydroxyethyl)aminotris(hydroxymethyl)methane; CaM, calcium-saturated recombinant chicken calmodulin; DSS, 2,2-dimethyl-2-silapentane-5-sulfonate; IPTG, isopropyl β-D-thiogalactopyranoside; NMR, nuclear magnetic resonance; smMLCKp, calmodulin recognition peptide from smooth muscle myosin light chain kinase.

10.1021/bi011818f CCC: $22.00
Published on Web 01/30/2002

though it is predominantly an unstructured random coil in the free state (*9*−*11*). The intermolecular interface is characterized by extensive interactions between methionine residues of calmodulin and hydrophobic groups of the bound domain and between glutamic acid side chains of CaM and basic groups of the bound domain. Structural variations around this basic theme have been subsequently observed (*9*−*11*, *13*−*17*).

Though a great deal is known about the structural endpoints of the molecular recognition process, much less is known about how calmodulin initially recognizes a target domain, how it collapses from an initial encounter complex to the final compact state, or the energetics of these events and associated structural changes. Hydrogen exchange methods in principle allow access to the equilibrium manifold of states and have been employed to probe the energetics and structural forms involved in molecular recognition by calmodulin (*18*). Here hydrostatic pressure is combined with hydrogen exchange methods to probe the energetics of the CaM·smMLCKp complex. The potential pressure sensitivity of the stability of ion pair interactions has been exploited previously to probe the role of ion pairs in the equilibrium structure of a complex involving apocalmodulin (*19*). Pressure perturbation of the manifold of states available to the CaM·smMLCKp complex is used to discover the nature of ion pair formation in the molecular recognition process. The working model presented by Ehrhardt et al. (*18*) implicitly requires the concerted formation of a number of ion pairs during a major structural reorganization leading to the final compact structure. Residue-specific information is gathered from the pressure dependence of the amide hydrogen exchange behavior of the smMLCKp domain bound to calmodulin. Both the magnitudes and pattern of apparent free energy changes and corresponding volume changes associated with hydrogen exchange in the bound domain are consistent with concerted formation of ion pairs between calmodulin and the target domain. These observations reinforce a central component of the working model for molecular recognition by calmodulin (*18*).

MATERIALS AND METHODS

Protein Purification and Sample Preparation. Recombinant chicken calmodulin was prepared in a manner similar to that described previously (*20*, *21*). Briefly, overexpression of the chicken CaM gene was performed in *E. coli* BL21-(DE3) cells grown on minimal media, followed by purification using phenyl-Sepharose affinity chromatography (*22*−*24*). The DNA encoding the smMLCKp sequence and employing codon usage optimal for expression in *E. coli* was subcloned from a previously described fusion protein expression system (*25*), and inserted into a modified pET-32b vector (Novagen) using standard methods. This vector contains the IPTG-inducable T7 promoter and thioredoxin fusion protein (*26*) and was used to transform *E. coli* BL21-(DE3) cells. The final smMLCKp peptide sequence, GSAR-RKWQKTGHAVRAIGRLS, includes a vestigial N-terminal Gly-Ser that is retained after thrombin digestion of the thioredoxin−smMLCKp fusion protein. This is the result of utilizing a *Bam*HI restriction site within the thrombin cleavage site of the vector. For overexpression of [^{15}N]- and [^{13}C,^{15}N]-labeled thioredoxin−smMLCKp fusion proteins, cells were grown on minimal media containing 0.1% $^{15}NH_4$-Cl (Isotech) with 0.2% of either unlabeled D-glucose (Sigma-Aldrich) or [U-$^{13}C_6$-99%]-D-glucose as the sole nitrogen and carbon sources, respectively. After 4 h induction by addition of 1 mM IPTG, cells were harvested, lysed by sonication, and clarified by centrifugation, followed by initial purification using a Ni−NTA His-bind column (Novagen). Thrombin cleavage of purified fusion proteins was performed in 50 mM NaCl, 20 mM Tris, 2.5 mM $CaCl_2$, pH 8.4; the cleaved mixture was immediately passed over a Q-Sepharose fast flow resin (Pharmacia). The smMLCKp peptide was collected in the flow-through and purified by C_8 reversed-phase chromatography (Vydack). Purity is typically >98% as analyzed by electrospray mass spectroscopy (Washington University, St. Louis). Routine yields of HPLC-purified peptide are 2.0 μmol (5 mg) per liter of cell growth.

The complex between smMLCKp and CaM was formed under dilute solution conditions, typically below 200 μM protein, to avoid excessive heat of reaction upon complexation (*22*), by titration of smMLCKp into a 15−25% molar excess of calmodulin. The molar excess of calmodulin ensures that the peptide is overwhelmingly in the bound state. The final concentration of labeled peptide in all NMR experiments was 2.0 mM, with CaM added in 10−20% excess (except where indicated in the text). Buffer conditions for assignments and hydrogen exchange experiments were 100 mM KCl, 20 mM Bis-Tris or imidazole, 20 mM $CaCl_2$, 0.02% NaN_3, with varied pH of 6.0−6.5, and 50−70% D_2O for hydrogen exchange experiments and 10% D_2O for assignment spectra.

NMR and Fluorescence Spectroscopy. Nuclear magnetic resonance spectra were recorded on Varian Inova spectrometers operating at 600 and 750 MHz (^{1}H), using a standard Varian 5 mm triple-resonance probe with 3-axis pulse field gradients. Proton chemical shifts were referenced to an external standard of DSS in D_2O; ^{13}C and ^{15}N chemical shifts were determined from the ^{1}H chemical shift of DSS using the ratio method of Sykes and co-workers (*27*). For all experiments, the ^{1}H carrier frequency was set to the water resonance. The sample temperature was set to 303 K. Complete backbone resonance assignments were based on the following NMR experiments: (1) ^{1}H-^{15}N HSQC (*28*, *29*); (2) ^{1}H-^{13}C constant-time HSQC (*30*); (3) CBCA(CO)NH (*31*, *32*); (4) HNCACB (*32*, *33*); (5) HNCO (*32*, *34*); (6) HN-(CA)CO (*35*); and (7) ^{15}N-edited 3D NOESY (*29*). All 3D experiments were recorded with common carrier frequencies and spectral widths. The 3D NOESY data were recorded with a mixing time of 80 ms. Quadrature detection in the indirect time domain was accomplished using the method of States et al. (*36*). ^{15}N-resolved experiments employed *z*-axis pulsed-field gradient sensitivity enhancement (*28*, *37*, *38*). Solvent suppression was achieved in all experiments with H_2O flip-back pulses and pulsed-field gradients (*29*, *39*). All NMR spectra were processed using the software package FELIX (Molecular Simulations Inc.).

Hydrogen exchange rates were determined using ^{1}H-^{15}N HSQC spectra (*28*, *29*) collected serially up to 4000 min, as required. The length of each individual experiment varied between approximately 10 and 80 min (8−64 scans per free induction decay, respectively). Samples were prepared by one of two methods; either by hydrating lyophilized CaM·[^{15}N]-smMLCKp complex with H_2O in a volume equivalent to 30−50% of the final volume, or by concentrating samples

to 30% final volume via centricon filters. After 30 min of equilibration, the hydrogen exchange reaction was initiated by dilution of the sample with D_2O buffer, bringing the final solutions to 50−70% D_2O. Observed hydrogen exchange (k_{obs}) rates were determined from amide cross-peak intensities fit to a monoexponential decay as described previously (*40*).

Under the EX2 condition of amide hydrogen exchange, the effective equilibrium constant for hydrogen bond breaking (K_{op}) or its inverse, the protection factor, can be obtained from k_{obs} and the intrinsic rate of exchange (k_{chem}) using eq 1 (*41*, *42*). The intrinsic rate of exchange for a given amide was calculated using the empirical corrections for sequence and solution conditions (isotope content, pH, temperature, pressure) (*43*−*45*). The effective local stability for the hydrogen bond is then determinable by eq 2.

$$k_{obs} = \frac{k_{op}k_{chem}[cat]}{k_{cl} + k_{op} + k_{chem}} \approx \left(\frac{k_{op}}{k_{cl}}\right)k_{chem}[cat] = K_{op}k_{chem}[cat] \quad (1)$$

$$\Delta G^{eff}_{HX} = -(RT)\ln K_{op} \quad (2)$$

High-pressure NMR experiments were performed with an apparatus that utilizes a high-pressure NMR tube technique that allows modern NMR experiments to be performed in a standard triple-resonance probe without modifications (*19*, *46*). The 5 mm single-crystal sapphire NMR tube is fitted in a BeCu charging valve with hydraulic pressurization applied via a hand-driven pump system. The advantages of using a high-pressure NMR tube in a standard NMR probe over modified high-pressure probe designs include full triple-resonance capability, narrow line widths (0.5 Hz ^{1}H), tunable pressure, quick assembly, and low sample volumes. The nominal sample volume used in hydrogen exchange experiments was 100 μL; samples were separated from the water used to transmit pressure by a layer of mineral oil. High-pressure fluorescence spectroscopy was carried out in a Jobin Yvon Spex Fluorolog 3 spectrofluorometer using a ISS high-pressure cell equipped with sapphire windows.

RESULTS

Sample Preparation and NMR Assignments. Previous studies from our group describing the interaction between the smMLCKp domain and CaM typically utilized peptides derived from chemical synthesis (*9*, *18*, *20*, *47*). In those studies, the smMLCKp peptide was isotropically enriched only at selected sites. To increase the completeness and robustness of the peptide models used, we have subsequently employed fusion-based recombinant expression of the small target domains to allow for uniform isotopic enrichment (*19*, *25*). The product resulting from thrombin cleavage of the thioredoxin−smMLCKp results in an N-terminal Gly-Ser dipeptide that is not part of the consensus calmodulin-binding sequence (*48*−*50*). Since we do not generally observe amide resonances for these two residues (see below) and they are not typically present in smMLCKp substrates used in other studies, we have elected to employ a numbering system that begins with the first alanine residue of the peptide, matching the previously reported proton assignments of the CaM·smMLCKp complex (*9*, *20*). Also, since the peptide used here was produced biosynthetically, the final product is not N-terminal acetylated or C-terminal amidated.

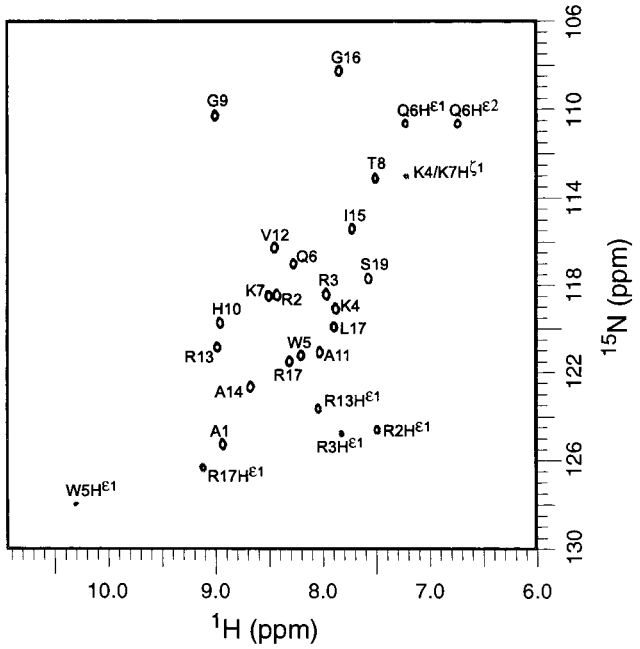

FIGURE 1: ^{1}H-^{15}N HSQC footprint of the CaM·[^{15}N]smMLCKp complex, with assignments of smMLCKp resonances indicated. The spectrum as shown was collected at 30 °C, pH 6.0, ambient pressure in the presence of 100 mM KCl, 20 mM Bis-Tris, and 20 mM $CaCl_2$ (10% D_2O). The cross-peaks corresponding to the side chain H^{ϵ} amide protons of the four arginines and the H^{ζ} amino protons of either Lys4 or Lys7 are folded in this spectrum.

Backbone resonance assignments of [^{13}C,^{15}N]-smMLCKp bound to Ca^{2+}-saturated calmodulin were completed using standard assignment strategies (Materials and Methods). Briefly, using three-dimensional HNCACB, CBCA(CO)NH, HNCO, and HN(CA)CO spectra, complete backbone assignments were determined for all peptide residues except for the N-terminal Gly-Ser dipeptide portion of the sequence. The assignments, summarized in Figure 1, have been deposited in the BioMagRes Bank (BMRB accession no. BMRB-5153). The fact that no backbone amide resonances are observed for the Gly-Ser dipeptide under these conditions is perhaps not unexpected given that these residues should be unstructured in the CaM·smMLCKp complex (*11*) and may therefore be exchange-broadened in addition to loss of intensity due to chemical exchange of the attached protons. At lower pH, where hydrogen exchange rates are slowed, the amide cross-peak of the first serine is observed, though the glycine is not (not shown). The chemical shifts of the current complex correspond well to those seen in the complex with the synthetic smMLCKp peptide lacking the GS N-terminal extension and having N- and C-terminal blocking (*9*, *20*). Helical NOE patterns in smMLCKp observed in these previous structural investigations of this system were verified using a 3D ^{15}N NOESY−HMQC spectrum (not shown). Analysis of NOE patterns, chemical shifts (*51*−*53*), and hydrogen exchange (see below) suggests that the carbonyl oxygens of the additional N-terminal residues participate in helical hydrogen bonding.

Native State Hydrogen Exchange. Using peak intensities derived from serially acquired ^{1}H-^{15}N HSQC spectra, hydrogen exchange rates could be measured at pH* 6.0, 25 °C, and ambient pressure for 11 of 19 observable backbone amide correlations (Figure 2, Table 1). The range of measurable amide hydrogen exchange rates for the [^{15}N]-

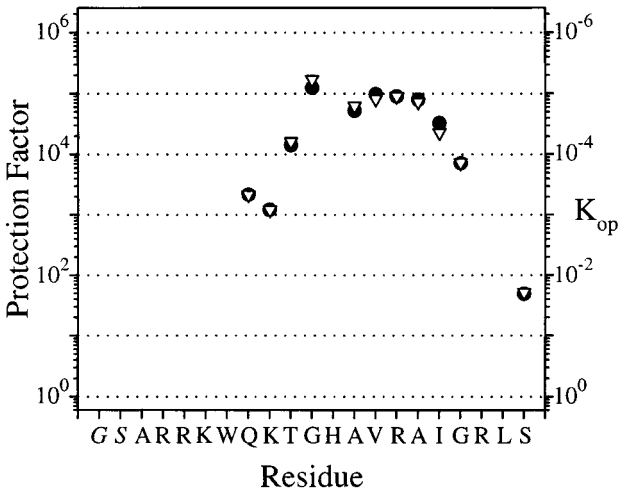

FIGURE 2: Hydrogen exchange profiles for backbone amide hydrogens of the smMLCKp peptide bound to calcium-saturated calmodulin. Protection factors (left ordinate) and K_{op} (right ordinate) versus sequence position are shown for a 1 mM complex of CaM·[^{15}N]-smMLCKp (1.15:1 molar ratio) in the presence of either 6 mM $CaCl_2$ (▽) or 50 mM $CaCl_2$ (●), corresponding to roughly 1 mM excess and a 10-fold excess of free Ca^{2+}, respectively.

Table 1: Pressure Dependence of Hydrogen Exchange in the smMLCKp Domain Bound to Calcium-Saturated Calmodulin[a]

residue[b]	K^0_{HX} ($\times 10^{-5}$)	ΔG^0_{HX} (kcal mol^{-1})	ΔV^0_{HX} (mL mol^{-1})	r^2 (n)
Thr8	0.16	5.7 (±0.3)	−53 (±5)	0.986 (6)
Gly9	3.9	7.6 (±0.2)	−80 (±4)	0.948 (10)
Ala11	0.51	6.4 (±0.3)	−73 (±6)	0.912 (8)
Val12	4.6	7.7 (±0.4)	−84 (±10)	0.982 (9)
Arg13	0.36	6.2 (±0.3)	−78 (±5)	0.939 (9)
Ala14	0.17	7.1 (±0.2)	−68 (±4)	0.937 (12)
Ile15	0.60	6.5 (±0.4)	−71 (±7)	0.970 (13)
Gly16	0.093	5.4 (±0.3)	−63 (±5)	0.898 (8)

[a] K^0_{HX}, ΔG^0_{HX}, and ΔV^0_{HX} values are obtained from linear fits of the K_{op} values determined at various hydrostatic pressures, at 25 °C. The number (n) of pressures used and the Pearson coefficient of correlation for the linear regression (r^2) are also shown. Error estimates of ΔG^0_{HX} values are determined from the regression analysis. Individual K_{op} values are calculated from measured hydrogen exchange rates (k_{obs}) divided by the predicted intrinsic rate of chemical exchange (k_{chem}). Calculation of k_{chem} included consideration of sequence, solvent isotope, pH, temperature, and pressure [see Fuentes and Wand (*46*)] and includes a correction for the ΔpH of Bis-Tris, using 3.1 mL/mol for the $\Delta V°$ of buffer ionization (*44*). Individual k_{obs}, k_{chem}, and K_{op} values for each residue at each pressure are listed in Table 1 of the Supporting Information. [b] Numbering adjusted to conform to the previous smMLCKp peptide sequence [see Ehrhardt et al. (*18*)]. Hydrogen exchange rates could not be measured at a sufficient number of pressures to obtain accurate K^0_{HX}, ΔG^0_{HX}, and ΔV^0_{HX} for Gly(−2), Ser(−1), Ala1, Arg2, Arg3, Lys4, Trp5, Gln6, Lys7, His10, Arg17, Lys18, and Ser19.

smMLCKp domain bound to CaM ranged from 0.03 min^{-1} (Gln6) to 0.0007 min^{-1} (Val12). Under these conditions, hydrogen exchange rates for A1-W5, H10, R17, and L18 are too rapid to measure by the method of serial acquisition of HSQC spectra. Exchange rates for Q6, K7, and S19 are only measurable at ambient pressure in a standard 5 mm NMR tube. The fact that the exchange rate of His10 is too fast to observe under these conditions is the result of protonation of the His10 imidazole ring (in the free state, see below) and a corresponding acceleration of the intrinsic chemical exchange rate. The presence of the so-called EX2 limit was confirmed by variation of pH and temperature (not shown). To confirm that the observed hydrogen exchange arises dominantly from the bound state and not from the free dissociated state of the peptide, the rates of exchange were measured at smMLCKp:CaM molar ratios of 1:1.2 and 1:2.5. The resulting exchange rates were essentially identical as was found previously (*18*), indicating a negligible contribution of the free (dissociated) state of the domain to the measured hydrogen exchange. A similar exercise was carried out for calcium using Ca^{2+}:CaM molar ratios of ∼6:1 and 50:1 with similar results (Figure 2). The importance of verifying the lack of any exchange rate-dependence on either free peptide or variable Ca^{2+} concentration is that, to probe dynamics of bound smMLCKp peptide, the measured rates must arise from events occurring in the bound state(s) (*18*). These results indicate that the observed rates are dominated by exchange arising from a CaM-bound conformation, not from a dissociated peptide state, under all conditions explored here.

Effective equilibrium constants were determined for the 11 smMLCKp residues with observable hydrogen exchange rates (Figure 2, Table 1) according to the empirical factors of Bai et al. (*43*). The distribution of protection factors ($1/K_{op}$) indicates a pattern that is characteristic of a helix. Residues in the first and last helical turns have a gradient of increasing stability away from the helical boundaries. This pattern matches the expected distribution of helix propensities predicted from helix−coil theory, noting that the amide H^Ns of the first four residues of an α-helix do not participate in a main chain hydrogen bond. Though no protection factors could be determined for the first seven residues, NOEs are observed from the amide proton of Trp5 to H^α and H^β protons of Lys4. Also, a weak NOE is observed from Lys4H^N to Arg3H^α along with a strong NOE observed between Lys4H^N to water; no NOE peaks are observed for residues N-terminal of Lys4. These observations are consistent with Ala1 or Arg2 being the first residues of the smMLCKp peptide in a helical conformation and the amide of Trp5 being the first to be hydrogen-bonded.

There are several minor differences between the results obtained previously with the chemically synthesized smMLCKp peptide (*9*, *18*) and the results described here using the recombinant domain. The additional Gly-Ser present in the recombinant peptide apparently extends the helical boundary by one residue relative to the synthetic peptide. Furthermore, the protection factors of the recombinant peptide (Figure 3) are uniformly smaller by a factor of ∼10 than seen for the synthetic peptide, corresponding to a difference of 1−1.5 kcal/mol in ΔG_{HX}. This additional stability corresponds closely to the effects of N- and C-terminal blocking on the stability of the α-helix (*54*−*56*). In addition, the presence of a charged C-terminal carboxyl group decreases k_{chem} sufficiently to allow the amide of Ser19 to be observed. The above results obtained at ambient pressure largely recapitulate the results of Ehrhardt et al. (*18*) and serve as a starting point for the current study.

Pressure Dependence of Hydrogen Exchange. The physical origin of "opening" events that result in exchange of amides in the high-affinity CaM·smMLCKp complex is of central interest to the current work. Over the past decade, it has become clear that hydrogen exchange phenomena in proteins can arise from a potentially complicated superposi-

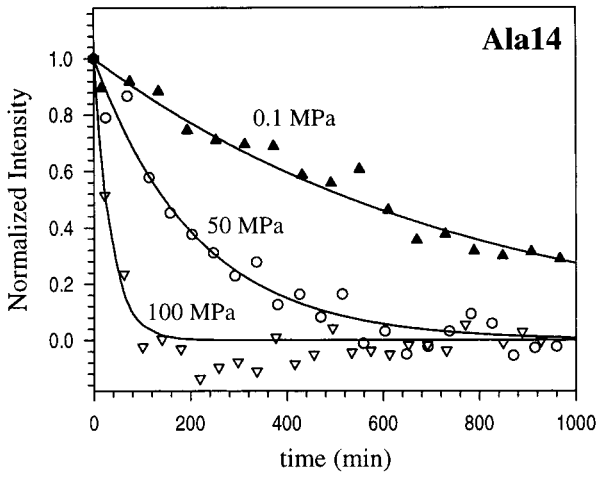

FIGURE 3: Amide hydrogen exchange of the CaM·smMLCKp complex as a function of applied hydrostatic pressure. Shown are representative amide hydrogen exchange curves for Ala14 of the bound smMLCKp domain at ambient pressure (0.1 MPa), 50 MPa, and 100 MPa.

tion of distinct physical events that lead to breakage of hydrogen bonds and exposure of amide hydrogens to solvent (*57*−*60*). Deconvolution of these various contributions to hydrogen exchange at a given amide site is often made possible by use of perturbation of the manifold of structural states of the protein in a way that identifies and distinguishes one state from another. Initially, perturbation using chemical denaturant and, to lesser extent, temperature was employed for this purpose (e.g., *40*, *61*−*66*). More recently, it has been illustrated that hydrostatic pressure is also a useful perturbant and provides highly complementary information about the nature of the equilibrium underlying hydrogen exchange phenomena (*40*, *46*). Here pressure is particularly useful since it has the unique potential of selectively destabilizing (detecting) ionic interactions in a background of extensive interactions not involving explicit charge (hydrogen bonding; hydrophobic van der Waals' interactions) (*19*).

The change in the free energy between two pressures, p_0 and p_1, is formally expressed as

$$\Delta G(p_1) = \Delta G(p_0) + \int_{p_0}^{p_1} \Delta V \, dp \qquad (3)$$

In the absence of an explicit functional form for the pressure dependence of a particular system, eq 3 is usually expressed by a Taylor series expansion about the reference pressure, p_0. For small dp:

$$\Delta G(p_1) = \Delta G^\circ(p_0) + (\Delta V^\circ)(\Delta p) + \frac{1}{2}(\Delta p)^2\left(\frac{d\Delta V^\circ}{dp}\right) + \frac{1}{6}(\Delta p)^3\left(\frac{d^2\Delta V^\circ}{dp^2}\right) + \ldots \qquad (4)$$

where ΔG° and ΔV° are the standard molar quantities of the system at the reference pressure, p_0, and $\Delta p = (p_1 - p_0)$. The second-order term arises from the difference in isothermal compressibility between the two states ($\Delta\kappa$) and is defined as $(-\partial\Delta V/\partial p)_T$. The third-order term arises from the pressure dependence of the differential isothermal compressibility, d$\Delta\kappa$/dp. When ($\Delta\kappa$) and d$\Delta\kappa$/dp are small, the dependence of ΔG° on pressure is first-order, and eq 4 reduces to

$$\Delta G(p_1) = \Delta G^\circ(p_0) + (\Delta V^\circ)(p_1 - p_0) \qquad (5)$$

The effect of applied hydrostatic pressure on the ^{1}H-^{15}N HSQC spectra of the smMLCKp·CaM complex is minor, producing only small variations in chemical shift at the highest pressures used for NMR spectroscopy (100 MPa). Fluorescence emission spectroscopy confirmed that the peptide did not dissociate at pressures as high as 300 MPa (the limit of the apparatus) and at concentrations as low as 100 nM (the limit of detection in the high-pressure cell). The K_d of the peptide was estimated by dilution to be less than 10 nM at ambient pressure.

Due to the relatively small active volume of the sapphire NMR tube, the signal intensity is reduced by an order of magnitude relative to a standard 5 mm NMR tube. As a result, the minimal length of time required is roughly 45 min per individual HSQC in order to obtain data of sufficient quality to permit determination of hydrogen exchange rates; optimal data collection requires roughly 80 min per HSQC. Even with additional signal averaging, the precision of the hydrogen exchange data is not as high as one typically observes for hydrogen exchange experiments. In the previous application of this high-pressure NMR system to studies of amide hydrogen exchange in the protein apocytochrome b_{562} (*46*), the problem of low signal intensity was in part overcome by increasing the protein concentration to 4 mM. The CaM·smMLCKp complex is limited to a maximum concentration of 2 mM due to aggregation of the complex at higher concentrations.

The effect of pressure on the rate of hydrogen exchange is significant. Representative hydrogen exchange curves for Ala14 of the bound smMLCKp peptide are shown in Figure 4. Increasing hydrostatic pressure leads to an increase in the observed rate of hydrogen exchange. Over the full range, the observed exchange rate increases by a factor of 15, while the chemical exchange rate (k_{chem}) for this residue increases by a factor of 1.45. A total of 18 separate experiments were conducted at 13 different pressures ranging from ambient pressure up to 100 MPa (Figure 4). Replicate measurements made at ambient pressure, 10 MPa, and at 50, 80, and 100 MPa allowed for estimation of the precision of the obtained rates. The confidence intervals in the fitted free energies for individual experiments (Table 1) are representative of the true accuracy as determined by replicate experiments. Note that amide exchange rates are not determined for every residue at every pressure; for example, the observed amide exchange rate of Thr8 is too rapid to be accurately measured above 50 MPa. Fits of the data to eq 4 indicate a linear dependence of the free energy, ΔG_{HX}, over the entire pressure range. A linear dependence on pressure suggests that a single equilibrium process dominates the response of this system to pressure and that the higher order terms in eq 4 are negligible over the pressure range used. Independent fits to the data in Figure 4 indicate a common ΔV_{HX} value of −74 (±6) mL/mol for the "plateau" region, the stretch of residues from G9 to G16, with a somewhat reduced ΔV_{HX} value of −53 (±5) mL/mol for Thr8 (Table 1). The pressure dependence of individual ΔG_{HX} values is shown in Figure 4. At the highest pressure employed, the residue-specific

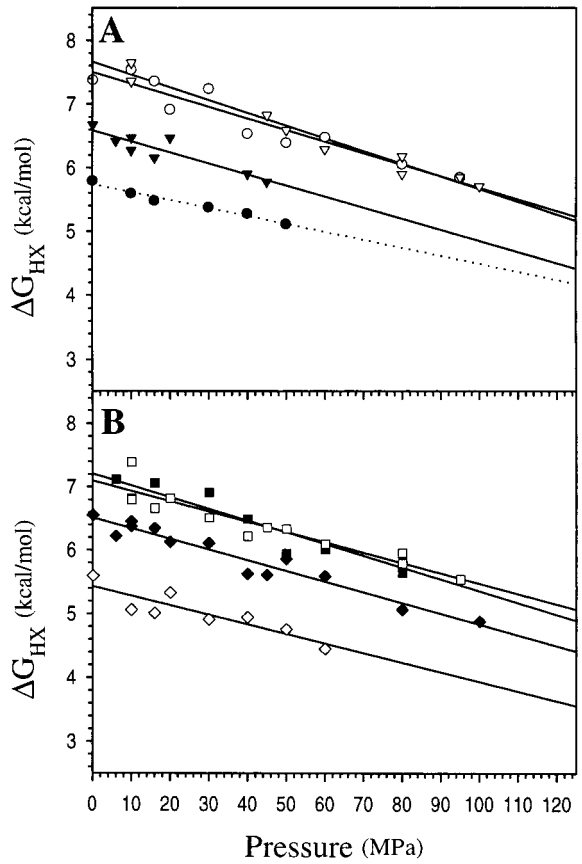

FIGURE 4: Pressure dependence of ΔG_{HX} of individual residues of the smMLCKp domain bound to CaM. Lines correspond to fits of the pressure dependence to eq 5. Solid lines correspond to residues with equivalent fitted ΔV°_{HX} values, within error. The dotted line represents the fit of ΔG°_{HX} for Thr8, the only residue with a significantly different ΔV°_{HX}. For clarity, the data have been separated into two panels: (panel A) residues Thr8 (●), Gly9 (○), Ala11 (▼), and Val12 (▽); (panel B) residues Arg13 (■), Ala14 (□), Ile15 (◆), and Gly16 (◇).

stabilities for the "plateau" region are decreased on average by 1.8 kcal/mol, or roughly a 25% destabilization of the total stability of these residues measured at ambient pressure. The profile of protection factors that is present at ambient pressure (Figure 2) persists at all pressures, denoting an approximately uniform response of the smMLCKp amide exchange to applied hydrostatic pressure.

DISCUSSION

Basic principles of thermodynamics require that ensembles of macromolecules sample not only their lowest free energy state, but also all possible higher energy states with some finite probability. Just as proteins fold and unfold in solution, macromolecular complexes cycle through bound and free conformations as well as all other states accessible to the individual molecules. Hydrogen exchange techniques are grounded in the fact that exchange generally occurs from those high-energy conformations that are populated according to Boltzmann factors, though they represent only a small fraction of the total population of the system. These minor forms are invisible to most experimental techniques but can be detected by hydrogen exchange because the dominant (hydrogen-bonded) state is hydrogen exchange incompetent and therefore does not contribute to the observed rate of exchange.

In the current application of hydrogen exchange to the problem of target recognition by calmodulin, we focus on the ensemble of states leading to exchange of smMLCKp amide hydrogens while bound to the calcium-saturated calmodulin. The NMR data describing the CaM·smMLCKp complex indicate the peptide is bound in an α-helical conformation (*9*, *11*). The majority of amide protons are involved in hydrogen bonds throughout the smMLCKp sequence; amides for the first several residues are solvent-exposed. This is consistent with our observations (Figure 2), as well as our previous hydrogen exchange studies of this CaM−peptide complex (*18*), that the rates of hydrogen exchange for the first six residues are rapid with protection factors that approach unity. Protection factors for the hydrogen-bonded amide protons at the ends of the helical segment are on the order of 10^3-10^4, corresponding to residue-specific stability constants on the order of 5 kcal/mol (Figure 5 and Table 1). The largest protection factors for smMLCKp amides are on the order of 10^5, comprising a "plateau" region in the center of the helix from Gly9 to Ile15. The residue-specific stability, ΔG_{HX}, for these residues is on the order of 7 kcal/mol. The decrease in slowing factors on the N- and C-terminal sides of residues in the plateau region is observed to be relatively smooth and occurs over a relatively small range, decreasing on average by a factor of 2.5 per residue, a value consistent with a highly solvated helix (*67*) but not with a well-packed helix that is an integral unit of secondary structure, where increments on the order of factors of 10 per residue are often seen. In apparent contradiction, however, the protection factors of the residues at the helical termini (10^4) are inconsistent with a free highly solvated peptide. These basic features were invoked to support the model proposed by Ehrhardt et al. (*18*) shown in Figure 6. The model is further supported by the observation that the D-amino acid analogue of smMLCKp binds avidly to calmodulin as a left-handed α-helix but does not permit collapse (*68*). The model predicts that general nonspecific or transient interactions between the (random coil) peptide and the surface of CaM induce helicity, via classical helix−coil transitions, in the bound domain but that simultaneous ion pair formation, not possible in the D-amino acid analogue, is required for collapse to the final compact complex structure. In addition, kinetic studies (*69*−*72*) indicate a two-phase process that would be consistent with rapid formation of the initial "open" encounter complex and slower conversion, involving concerted ion pair formation to the final structure.[2]

In the current study, we elected to use pressure to detect the presence of a state of the bound domain that arises from the formation of a large amount of charge, i.e., to test for the large-scale structural reorganization involving concerted ion pair formation suggested by Figure 6. This approach relies on the phenomenon of electrostriction where solvation of ions by water can often result in a significant decrease in system volume (*73*, *74*). Thus, an equilibrium between an intimate ion pair, which is polar but not explicitly charged, and its separated and individually solvated charged compo-

[2] The terms "open" and "closed" should not be confused with their use to describe the relative orientation of helices in EF-hands. Here "closed" refers to the final compact structure of the complex seen, for example, in the crystal structure (*11*) while "open" refers to the state(s) enclosed in parentheses in Figure 6.

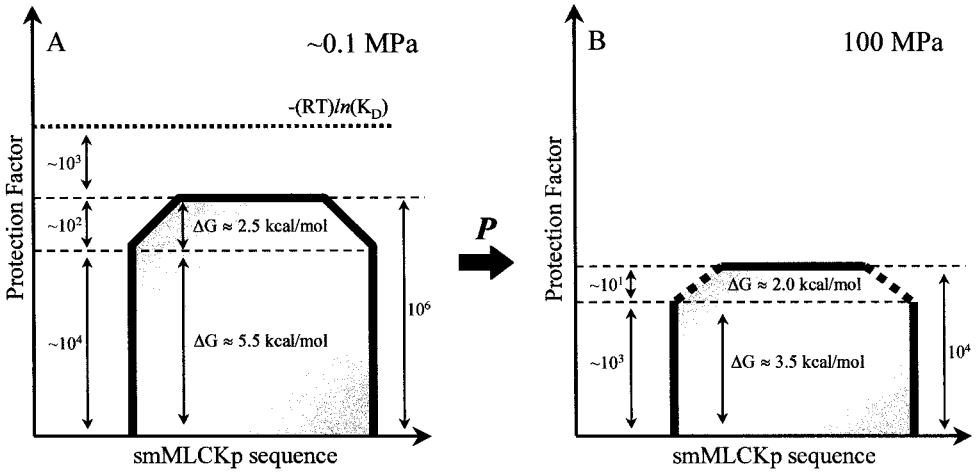

FIGURE 5: Schematic illustration of the profile of hydrogen exchange in smMLCKp bound to CaM at ambient pressure (panel A) and 100 MPa (panel B). The topmost line indicates the expected binding free energy based on spectroscopic measurements, where $K_d \sim 10^{-9}$ M.

nents is pushed to the dissociated state by application of hydrostatic pressure. In contrast, disruption of interactions not involving explicit charges (e.g., hydrogen bonds) generally does not result in significant electrostriction. This provides a route for the molecular dissection of ion pair interactions from other types of interactions (*19*).

The model outlined in Figure 6 would predict a large negative volume change due to electrostriction associated with disruption of the ion pairs involved at the interface between the domain and calmodulin in the compact "closed" complex upon transition to the "open" structure. A concerted transition, which would entail simultaneous disruption of the ion pairs, would be manifested uniformly across all residues involved in that transition. The effect of applied hydrostatic pressure on peptide hydrogen exchange is a general acceleration of the observed exchange rate for each amide indicating a pressure-induced shift in the overall equilibrium toward the hydrogen-exchange competent states. Individual fits of ΔG_{HX} values as a function of pressure indicate the effective stabilities of smMLCKp amides vary linearly with pressure (Figure 4 and Table 1). This simplifies considerably the interpretation of the pressure dependence. Importantly, residues in the core of the bound helical domain are uniformly affected by pressure and have an average ΔV_{HX} value of -74 (± 6) mL/mol. The uniformity, sign, and magnitude of the volume change are consistent with the simultaneous disruption of 2−4 ion pairs during the structural transition. On this basis alone, there is some ambiguity in the number of ion pairs involved since the volume change associated with electrostriction arising from separated ion pairs is variable. Nevertheless, the magnitude of the observed volume change is simply too large to arise solely from nonionic interactions, which are generally found to involve volume changes an order of magnitude or more smaller (*73*). Furthermore, the observed volume change is quite similar to that observed for a pressure-induced structural transition in a complex between apocalmodulin and the calmodulin-binding domain of neuromodulin (*19*). In that case, the change in free energy associated with the structural transition was small enough to allow for the transition to be directly monitored by NMR spectroscopy, which thereby allowed for an unequivocal demonstration that the disruption of two intermolecular ion pairs occurred.

The structural transition characterized by the cooperative loss of ion pairs and other intermolecular contacts between calmodulin and the bound domain is associated with a unimolecular (i.e., associated complex) equilibrium constant on the order of 10^{-4} ($\Delta G_{ip} \sim 5$ kcal/mol). The free energy change associated with this structural transition (ΔG_{ip}) is apparently the dominant contribution from calmodulin−domain interactions to the overall free energy of binding. Though the crystal structure of the CaM·smMLCKp complex does not reveal the charge state of ionizable groups at the interface, it does suggest the presence of two intermolecular interactions involving residues in the core of smMLCKp sequence. Lys7 and Arg13 (Arg17) of the peptide are close to the CaM side chains of E114 and E84, respectively (*11*). The chemical shifts and pH dependence of the stability of the complex (not shown) are both consistent with ion pairing between these groups. It is important to note that the chemical shifts of imidazole ring resonances of His10 of the smMLCKp domain indicate that it is not charged in the compact complex, consistent with its role in intermolecular hydrogen bonding rather than ion pairing.

The surface-associated helix−coil transitions of the bound domain span an ensemble of structures (the states enclosed by parentheses in Figure 6) that is characterized by an equilibrium constant on the order of 10^{-2} ($\Delta G_{hc} \sim 2$ kcal/mol). The apparent change in free energy measured by hydrogen exchange, ΔG_{HX}, is derived from the structural rearrangement associated with breaking of ion pairs, ΔG_{ip}, and loss of helical hydrogen bonds, ΔG_{hc}. The balance of the free energy of dissociation ($K_d^0 \sim 10^{-9}$) arises from formation of the initial encounter complex.

In summary, the results presented here are consistent with the multistep equilibrium outlined in Figure 6. The pressure sensitive step is associated with the loss of intermolecular ionic contacts and an opening (solvation) of the complex, as outlined above. Based on the structure of the CaM·smMLCKp complex, many of the contacts observed in the intermolecular interface would require the bound peptide to adopt a helical conformation in order to be formed (*11*).

While induction of an α-helical conformation is important for CaM association in the study of short recognition sequences, conformational transitions of whole targets accompanying CaM binding may be a general feature of

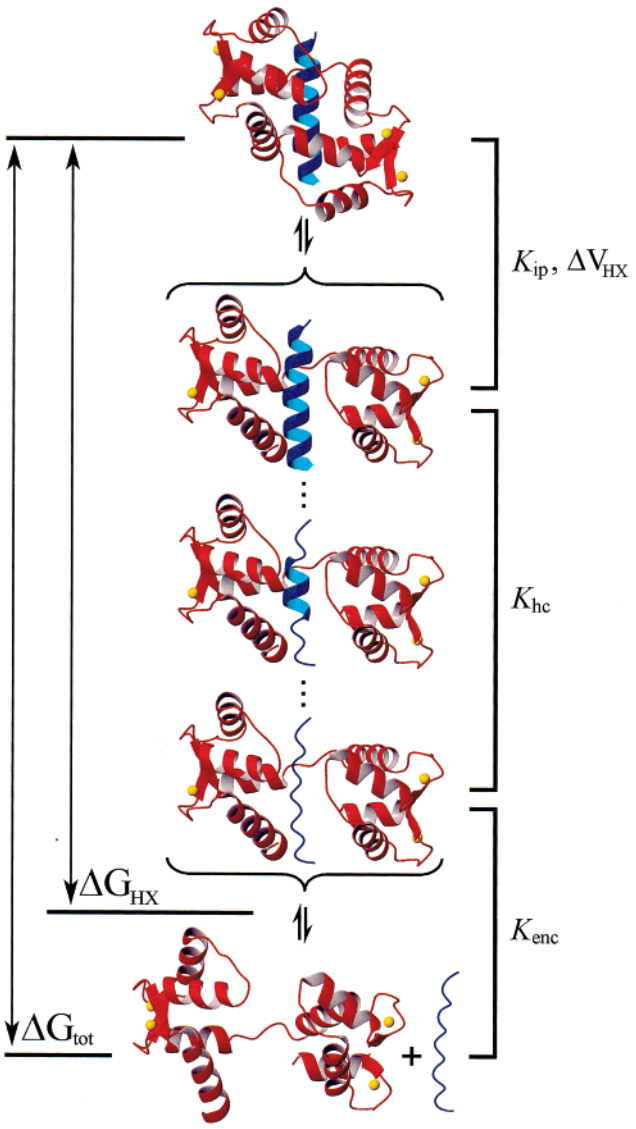

FIGURE 6: Illustration of a physical model for molecular recognition by calcium-saturated calmodulin (CaM) (red) of the smMLCKp domain (blue). The random coil smMLCKp domain associates with CaM, forming an initial encounter complex (K_{enc}). General surface and perhaps hydrophobic anchoring interactions promote helix formation on the surface of calmodulin, resulting in an "open" complex structure (K_{hc}). Upon completion of the core helical region of the bound smMLCKp domain, concerted ion pairing can occur, with formation of other types of intermolecular contacts, and lead to the final compact "closed" globular complex (K_{ip}). The final collapse occurs with a $\Delta V^{\circ}_{HX} \sim +74$ (± 6) mL/mol which is largely due to the loss of electrostriction of water upon formation of the intimate ion pairs (see text). Figures were prepared using MOLMOL (*80*) and employed the coordinates from Meador et al. (*9*−*11*), PDB code: 1cdl.

calcium-regulated activation. Though structural information on whole proteins that are regulated by calmodulin is sparse, in the case of the CaM-activated protein kinase I (CaMKI) the recognition sequence is not fully helical (*75*). In this system, the autoinhibitory sequence overlaps with the calmodulin recognition sequence, with the full regulatory sequence occluding the active site, thereby blocking substrate entry. The C-terminal portion of the CaM recognition sequence of this protein is partly helical though it is "random coil" around residue Trp303 (the important anchoring tryptophan) that is exposed to solvent. Two initial molecular recognition scenarios are therefore suggested. In one, CaM utilizes this exposed tryptophan as the initial recognition element, followed by the conformational rearrangements suggested by Figure 6 that result in the exposure of the active site of the kinase. Another mechanism could simply involve the autoinhibitory/CaM recognition sequence occasionally diffusing from the active site and entering the scheme outlined above. The analogies between the CaM·CaMKI system and the CaM·smMLCKp system can be easily drawn as the pseudosubstrate model is also apparently applicable to the smooth muscle myosin light chain kinase enzyme, from which the smMLCKp is derived. The pseudosubstrate sequence of smMLCK has been shown to overlap with the CaM recognition sequence (*76*), and replacement of the autoinhibitory sequence with a substrate sequence showed autophosphorylation in the absence of CaM (*77*).

The view provided by the hydrogen exchange studies described here is fundamentally thermodynamic in nature and, in the absence of additional constraints, cannot define the kinetic or temporal relationships between the various states identified (*78*, *79*). However, the biphasic kinetics observed for the binding of calmodulin-binding domains to CaM (*69*−*72*) would appear to support the temporal relationships suggested by Figure 6. The cooperativity of the structural transition, which is made apparent by the uniform pressure dependence, is ascribed to a concerted formation and subsequent burial of intermolecular ion pairs. Structurally, these ion pairings are made most likely by the presence of extensive α-helical structure. Hence it is natural to ascribe the fast kinetic phase of binding to passage from the initial encounter complex to the fully formed but highly solvent-exposed helical smMLCKp domain bound in an "open" complex. The relatively large barrier giving rise to the slower phase of binding would then be associated with the large-scale reorganization of the domains of calmodulin, intermolecular ion pair formation, and expulsion of water leading to the final compact "closed" complex structure.

SUPPORTING INFORMATION AVAILABLE

One table of observed hydrogen exchange rates, intrinsic chemical exchange rates, and effective opening constants for individual residues at various hydrostatic pressures. This material is available free of charge via the Internet at http://pubs.acs.org.

REFERENCES

1. Crivici, A., and Ikura, M. (1995) *Annu. Rev. Biophys. Biomol. Struct. 24*, 85−116.
2. O'Neil, K. T., and DeGrado, W. F. (1990) *Trends Biochem. Sci. 15*, 59−64.
3. James, P., Vorherr, T., and Carafoli, E. (1995) *Trends Biochem. Sci. 20*, 38−42.
4. Rhoads, A. R., and Friedberg, F. (1997) *FASEB J. 11*, 331−340.
5. Kuboniwa, H., Tjandra, N., Grzesiek, S., Ren, H., Klee, C. B., and Bax, A. (1995) *Nat. Struct. Biol. 2*, 768−776.
6. Zhang, M., Tanaka, T., and Ikura, M. (1995) *Nat. Struct. Biol. 2*, 758−767.
7. Babu, Y. S., Sack, J. S., Greenhough, T. J., Bugg, C. E., Means, A. R., and Cook, W. J. (1985) *Nature 315*, 37−40.
8. Barbato, G., Ikura, M., Kay, L. E., Pastor, R. W., and Bax, A. (1992) *Biochemistry 31*, 5269−5278.

9. Roth, S. M., Schneider, D. M., Strobel, L. A., VanBerkum, M. F., Means, A. R., and Wand, A. J. (1991) *Biochemistry 30*, 10078−10084.
10. Ikura, M., Clore, G. M., Gronenborn, A. M., Zhu, G., Klee, C. B., and Bax, A. (1992) *Science 256*, 632−638.
11. Meador, W. E., Means, A. R., and Quiocho, F. A. (1992) *Science 257*, 1251−1255.
12. Lo Conte, L., Chothia, C., and Janin, J. (1999) *J. Mol. Biol. 285*, 2177−2198.
13. Ikura, M., Barbato, G., Klee, C. B., and Bax, A. (1992) *Cell Calcium 13*, 391−400.
14. Meador, W. E., Means, A. R., and Quiocho, F. A. (1993) *Science 262*, 1718−1721.
15. Osawa, M., Tokumitsu, H., Swindells, M. B., Kurihara, H., Orita, M., Shibanuma, T., Furuya, T., and Ikura, M. (1999) *Nat. Struct. Biol. 6*, 819−824.
16. Elshorst, B., Hennig, M., Forsterling, H., Diener, A., Maurer, M., Schulte, P., Schwalbe, H., Griesinger, C., Krebs, J., Schmid, H., Vorherr, T., and Carafoli, E. (1999) *Biochemistry 38*, 12320−12332.
17. Larsson, G., Schleucher, J., Onions, J., Hermann, S., Grundstrom, T., and Wijmenga, S. S. (2001) *Protein Sci. 10*, 169−186.
18. Ehrhardt, M. R., Urbauer, J. L., and Wand, A. J. (1995) *Biochemistry 34*, 2731−2738.
19. Urbauer, J. L., Ehrhardt, M. R., Bieber, R. J., Flynn, P. F., and Wand, A. J. (1996) *J. Am. Chem. Soc. 118*, 11329−11330.
20. Roth, S. M., Schneider, D. M., Strobel, L. A., Van Berkum, M. F., Means, A. R., and Wand, A. J. (1992) *Biochemistry 31*, 1443−1451.
21. Urbauer, J. L., Short, J. H., Dow, L. K., and Wand, A. J. (1995) *Biochemistry 34*, 8099−8109.
22. Seeholzer, S. H., and Wand, A. J. (1989) *Biochemistry 28*, 4011−4020.
23. Putkey, J. A., Draetta, G. F., Slaughter, G. R., Klee, C. B., Cohen, P., Stull, J. T., and Means, A. R. (1986) *J. Biol. Chem. 261*, 9896−9903.
24. Gopalakrishna, R., and Anderson, W. B. (1982) *Biochem. Biophys. Res. Commun. 104*, 830−836.
25. Lee, A. L., Kinnear, S. A., and Wand, A. J. (2000) *Nat. Struct. Biol. 7*, 72−77.
26. Skalicky, J. J., Gibney, B. R., Rabanal, F., Bieber Urbauer, R. J., Dutton, P. L., and Wand, A. J. (1999) *J. Am. Chem. Soc. 121*, 4941−4951.
27. Wishart, D. S., Bigam, C. G., Yao, J., Abildgaard, F., Dyson, H. J., Oldfield, E., Markley, J. L., and Sykes, B. D. (1995) *J. Biomol. NMR 6*, 135−140.
28. Kay, L. E., Keifer, P., and Saarinen, T. (1992) *J. Am. Chem. Soc. 114*, 10663−10665.
29. Zhang, O. W., Kay, L. E., Olivier, J. P., and Forman-Kay, J. D. (1994) *J. Biomol. NMR 4*, 845−858.
30. Vuister, G. W., and Bax, A. (1992) *J. Magn. Reson. 98*, 428−435.
31. Grzesiek, S., and Bax, A. (1992) *J. Am. Chem. Soc. 114*, 6291−6293.
32. Muhandiram, D. R., and Kay, L. E. (1994) *J. Magn. Reson., Ser. B 103*, 203−216.
33. Wittekind, M., and Mueller, L. (1993) *J. Magn. Reson., Ser. B 101*, 201−205.
34. Kay, L. E., Xu, G. Y., and Yamazaki, T. (1994) *J. Magn. Reson., Ser. A 109*, 129−133.
35. Clubb, R. T., Thanabal, V., and Wagner, G. (1992) *J. Magn. Reson. 97*, 213-217.
36. Marion, D., Ikura, M., Tschudin, R., and Bax, A. (1989) *J. Magn. Reson. 85*, 393−399.
37. Cavanagh, J., and Rance, M. (1990) *J. Magn. Reson. 88*, 72−85.
38. Palmer, A. G., Cavanagh, J., Byrd, R. A., and Rance, M. (1992) *J. Magn. Reson. 96*, 416−424.
39. Grzesiek, S., and Bax, A. (1993) *J. Am. Chem. Soc. 115*, 12593−12594.
40. Fuentes, E. J., and Wand, A. J. (1998) *Biochemistry 37*, 3687−3698.
41. Hvidt, A., and Nielsen, S. O. (1966) *Adv. Protein Chem. 21*, 287−386.
42. Englander, S. W., and Kallenbach, N. R. (1983) *Q. Rev. Biophys. 16*, 521−655.
43. Bai, Y., Milne, J. S., Mayne, L., and Englander, S. W. (1993) *Proteins: Struct., Funct., Genet. 17*, 75−86.
44. Kitamura, Y., and Itoh, T. (1987) *J. Solution Chem. 16*, 715−725.
45. Connelly, G. P., Bai, Y., Jeng, M. F., and Englander, S. W. (1993) *Proteins: Struct., Funct., Genet. 17*, 87−92.
46. Fuentes, E. J., and Wand, A. J. (1998) *Biochemistry 37*, 9877−9883.
47. Chen, C., Feng, Y., Short, J. H., and Wand, A. J. (1993) *Arch. Biochem. Biophys. 306*, 510−514.
48. Kemp, B. E., Pearson, R. B., Guerriero, V., Jr., Bagchi, I. C., and Means, A. R. (1987) *J. Biol. Chem. 262*, 2542−2548.
49. Lukas, T. J., Burgess, W. H., Prendergast, F. G., Lau, W., and Watterson, D. M. (1986) *Biochemistry 25*, 1458−1464.
50. Pearson, R. B., Wettenhall, R. E., Means, A. R., Hartshorne, D. J., and Kemp, B. E. (1988) *Science 241*, 970−973.
51. Wishart, D. S., Sykes, B. D., and Richards, F. M. (1991) *J. Mol. Biol. 222*, 311−333.
52. Wishart, D. S., and Nip, A. M. (1998) *Biochem. Cell Biol. 76*, 153−163.
53. Wishart, D. S., and Sykes, B. D. (1994) *Methods Enzymol. 239*, 363−392.
54. Doig, A. J., and Baldwin, R. L. (1995) *Protein Sci. 4*, 1325−1336.
55. Shoemaker, K. R., Kim, P. S., York, E. J., Stewart, J. M., and Baldwin, R. L. (1987) *Nature 326*, 563−567.
56. Shoemaker, K. R., Kim, P. S., Brems, D. N., Marqusee, S., York, E. J., Chaiken, I. M., Stewart, J. M., and Baldwin, R. L. (1985) *Proc. Natl. Acad. Sci. U.S.A. 82*, 2349−2353.
57. Woodward, C. K. (1994) *Curr. Opin. Struct. Biol. 4*, 112−116.
58. Englander, S. W., Sosnick, T. R., Englander, J. J., and Mayne, L. (1996) *Curr. Opin. Struct. Biol. 6*, 18−23.
59. Englander, S. W., Mayne, L., Bai, Y., and Sosnick, T. R. (1997) *Protein Sci. 6*, 1101−1109.
60. Raschke, T. M., and Marqusee, S. (1998) *Curr. Opin. Biotechnol. 9*, 80−86.
61. Mayo, S. L., and Baldwin, R. L. (1993) *Science 262*, 873−876.
62. Bai, Y., Sosnick, T. R., Mayne, L., and Englander, S. W. (1995) *Science 269*, 192−197.
63. Bai, Y., and Englander, S. W. (1996) *Proteins: Struct., Funct., Genet. 24*, 145−151.
64. Chamberlain, A. K., Handel, T. M., and Marqusee, S. (1996) *Nat. Struct. Biol. 3*, 782−787.
65. Clarke, J., and Fersht, A. R. (1996) *Fold. Des. 1*, 243−254.
66. Hiller, R., Zhou, Z. H., Adams, M. W., and Englander, S. W. (1997) *Proc. Natl. Acad. Sci. U.S.A. 94*, 11329−11332.
67. Rohl, C. A., and Baldwin, R. L. (1994) *Biochemistry 33*, 7760−7767.
68. Fisher, P. J., Prendergast, F. G., Ehrhardt, M. R., Urbauer, J. L., Wand, A. J., Sedarous, S. S., McCormick, D. J., and Buckley, P. J. (1994) *Nature 368*, 651−653.
69. Török, K., and Whitaker, M. (1994) *Bioessays 16*, 221−224.
70. Török, K., and Trentham, D. R. (1994) *Biochemistry 33*, 12807−12820.
71. Török, K., Cowley, D. J., Brandmeier, B. D., Howell, S., Aitken, A., and Trentham, D. R. (1998) *Biochemistry 37*, 6188−6198.

72. Brown, S. E., Martin, S. R., and Bayley, P. M. (1997) *J. Biol. Chem. 272*, 3389−3397.
73. Distèche, A. (1972) *Symp. Soc. Exp. Biol. 26*, 27−60.
74. Morild, E. (1981) *Adv. Protein Chem. 34*, 93−166.
75. Goldberg, J., Nairn, A. C., and Kuriyan, J. (1996) *Cell 84*, 875−887.
76. Knighton, D. R., Pearson, R. B., Sowadski, J. M., Means, A. R., Ten Eyck, L. F., Taylor, S. S., and Kemp, B. E. (1992) *Science 258*, 130−135.
77. Bagchi, I. C., Kemp, B. E., and Means, A. R. (1992) *Mol. Endocrinol. 6*, 621−626.
78. Clarke, J., Itzhaki, L. S., and Fersht, A. R. (1997) *Trends Biochem. Sci. 22*, 284−287.
79. Englander, S. W. (1998) *Trends Biochem. Sci. 23*, 378−381.
80. Koradi, R., Billeter, M., and Wuthrich, K. (1996) *J. Mol. Graphics 14*, 51−55.

BI011818F